Application of the Reassigned Joint Time-Frequency Transform to Wideband Scattering From Waveguide Cavities

Shobha Sundar Ram and Hao Ling, *Fellow, IEEE*

***Abstract*—The wideband return from a circular waveguide cavity is investigated in the joint time-frequency space using the reassigned joint time-frequency (RJTF) transform. Equations for generating the reassigned joint time-frequency distribution from a frequency domain signal are presented. The performance of the reassigned transform is compared with that of the short-time Fourier transform (STFT) based on data obtained from both simulation and measurement.**

***Index Terms*—Radar scattering, reassigned joint time-frequency (RJTF) transform, short-time Fourier transform (STFT), waveguide cavities.**

I. Introduction

THE study of wideband scattering data from different structures is important for radar target identification. The wideband returns from an open-ended waveguide cavity have been investigated previously in the joint time-frequency domain [1]–[3]. It was found that the joint time-frequency space provides significant insights into many scattering mechanisms including scattering centers, resonances, and modal dispersions. The most widely used time-frequency representation is the short-time Fourier transform (STFT). A well-known limitation of the STFT is that the window width defines the precision of the signal in the time and frequency domains. For instance, if the time window in the STFT is σ, then the thickness of the signal along the time axis is σ and $1/\sigma$ along the frequency axis. Another well-known time-frequency representation, the Wigner–Ville distribution, shows excellent signal localization characteristics. However, additional cross terms are introduced in the time-frequency plane. In this letter, we investigate the application of the reassigned joint-time frequency transform on the broadband returns of an open-ended waveguide cavity.

The reassigned joint time-frequency (RJTF) transform, first developed by Kodera *et al.* [4], has been applied extensively in the acoustic community on speech and music signals [5]–[7]. In the resulting RJTF distribution, the signal is represented as a function of its instantaneous time (or local group delay) and instantaneous frequency. The main feature of this distribution is that it has optimum time-frequency localization properties without the presence of interference/cross terms. Simple signals such as tones, clicks, and chirps are concentrated to lines of infinite precision or zero thickness in the reassigned spectrogram. This contrasts with the performance of other time-frequency distributions such as the STFT.

Traditionally, the RJTF has been applied on time domain signals. However, the collected data from stepped frequency radars are usually in the frequency domain. Therefore, we first derive an expression for the reassigned spectrogram for a frequency domain signal. Our RJTF implementation is a dual to the form proposed in [7]. It is then applied to the broadband radar echo data obtained both by simulation and measurement.

Manuscript received July 20, 2007; revised October 16, 2007. This work was supported by the National Science Foundation under the Major Research Instrumentation Program and Grant CBET-0730924.

The authors are with the Department of Electrical and Computer Engineering, University of Texas at Austin, Austin, TX 78731 USA (e-mail: shobhasram@mail.utexas.edu).

Digital Object Identifier 10.1109/LAWP.2007.911391

II. Reassigned Joint Time-Frequency Transform

It is well known that the STFT can be applied to either a time domain signal $x(t)$ or its frequency domain representation $X(\omega)$ as shown in

$$\chi_1(t,\omega) = \int x(t')e^{-\frac{(t-t')^2}{2\sigma^2}}e^{+j\omega(t-t')}dt' = |\chi|e^{j\phi} \quad (1)$$

$$\chi_2(t,\omega)t = \frac{1}{2\pi}\int X(\omega')e^{-\frac{(\omega-\omega')^2\sigma^2}{2}}e^{-jt(\omega-\omega')}d\omega' = |\chi|e^{j\psi}. \quad (2)$$

Gaussian windows of time width σ and frequency width $1/\sigma$ have been used in the previous STFT definitions. Since the windows used in the two domains are Fourier transform pairs, the resulting STFT distributions are identical except for a phase factor $e^{-j\omega t}$.

The reassigned transform reassigns the STFT distribution to the instantaneous time and instantaneous frequency coordinates $(t_{\text{ins}}, f_{\text{ins}})$. They are derivable from the time and frequency derivatives of the phase ϕ of the STFT of a time domain signal. Different implementations of the phase derivatives have been discussed in literature. Here, we adopt the form presented in [7]. First, a second distribution $\eta_1(t,w)$ is defined using a time-window product as

$$\eta_1(t,w) = \frac{1}{\sigma}\int (t'-t)x(t')e^{-\frac{(t-t')^2}{2\sigma^2}}e^{jw}(t-t')\,dt'. \quad (3)$$

The instantaneous time t_{ins} and instantaneous frequency f_{ins} are then derived from the two distributions $\chi_1(t,w)$ and $\eta_1(t,w)$ as shown in

$$f_{\text{ins}} = \frac{1}{2\pi}\frac{\partial\phi}{\partial t} = f + \frac{1}{2\pi\sigma}\text{Im}\left\{\frac{\eta_1}{\chi_1}\right\} \quad (4)$$

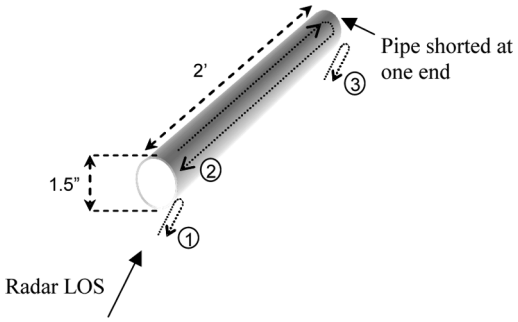

Fig. 1. Scattered field returns from an open-ended circular waveguide cavity.

$$t_{\rm ins} = t - \frac{\partial \phi}{\partial \omega} = t + \sigma {\rm Re}\left\{\frac{\eta_1}{\chi_1}\right\}. \tag{5}$$

In parallel with the previous derivation, we present a dual formula of the RJTF using the frequency domain signal. A second spectrogram $\eta_2(t,\omega)$ is defined using a frequency-window product as

$$\eta_2(t,\omega) = \frac{\sigma}{2\pi}\int (\omega' - \omega) X(\omega') e^{\frac{-(\omega-\omega')^2\sigma^2}{2}} e^{-jt(\omega-\omega')} d\omega'. \tag{6}$$

The instantaneous frequency and instantaneous time, which are related to the partial derivatives of the spectral phase ψ, can then be derived using distributions $\chi_2(t,\omega)$ and $\eta_2(t,\omega,)$ as follows:

$$f_{\rm ins} = f + \frac{1}{2\pi}\frac{\partial \psi}{\partial t} = f + \frac{1}{2\pi\sigma}{\rm Re}\left\{\frac{\eta_2}{\chi_2}\right\} \tag{7}$$

$$t_{\rm ins} = -\frac{\partial \psi}{\partial \omega} = t - \sigma {\rm Im}\left\{\frac{\eta_2}{\chi_2}\right\}. \tag{8}$$

Consequently, to generate the RJFT, each point (t,f) in the STFT spectrogram is first transformed to a corresponding point in the $(t_{\rm ins}, f_{\rm ins})$ plane using (7) and (8). A fine grid is then formed in the new plane. The strength of each cell in the grid is determined by the square root of the sum of the absolute strengths $|\chi|^2$ of all the points that fall within that cell. This operation ensures that the energy is conserved during the transformation of the distribution from the (t,f) plane to the $(t_{\rm ins}, f_{\rm ins})$ plane.

III. Broadband Radar Returns From a Circular Duct

We consider a 2-ft-long circular duct of 1.5-in diameter that is shorted at one end. The total backscattered field from the open-ended waveguide cavity consists of three dominant mechanisms as shown in Fig. 1. These include the diffraction from the rim of the open end of the cavity 1, the scattering contribution from the interior of the cavity 2, and the scattering from the exterior back end of the cavity 3. When the frequency of the incident field is above the lowest cutoff frequency of the waveguide, propagating modes are excited within the cavity.

The broadband returns of the duct are simulated from 1 to 18 GHz. The returns from the interior of the cavity are modeled using a modal approach [8] and the rim diffraction component is determined based on the asymptotic formula given in [9]. A small attenuation factor is introduced in the simulation to model wall losses and make the modes decay with time. The diffraction from the exterior of the cavity is not modeled in the simulation. Fig. 2(a) shows the STFT of the backscattered data at normal incidence. A Gaussian window of 1 GHz is used. Two scattering mechanisms are observed in the spectrogram. The nondispersive rim diffraction 1 is the first vertical line. This is the only component that is present below the cutoff frequency of the lowest $\rm TE_{11}$ mode in the waveguide. The scattering from the interior of the duct 2 is observed after a roundtrip delay of 4.1 ns. This consists of the dispersion curves of two waveguide modes $\rm TE_{11}$ (with a cutoff of 4.62 GHz) and $\rm TM_{20}$ (13.84 GHz), excited within the cavity. The thickness of the signals along the time and the frequency axes depend on the size of the window used in the STFT. The choice of the window size, however, causes a time and frequency domain tradeoff as it is not possible to simultaneously determine the precise time and the frequency location of each component in the distribution. Fig. 2(b) shows the reassigned distribution of the simulated data as a function of the instantaneous time and instantaneous frequency. Some important features are observed. The signal is now localized into very thin lines along *both* the time and the frequency axes. The thickness of the signals is independent of the choice of the window size used in the STFT and is instead fixed by the fine grid size in the $(t_{\rm ins}, f_{\rm ins})$ plane. The grid size is chosen sufficiently large here in order for the features to be recognizable in the plots. In all of our plots, the dynamic range is fixed at 50 dB where the high limit is set as the maximum value of the time-frequency distribution. Note that the peak value of the RJTF is about 14 dB higher than that of the STFT, due to improved localization of the features.

Fig. 3(a) shows the spectrogram generated by the application of the STFT on the simulated backscattering for a vertically polarized wave at 45° incidence. Many more modes are excited at this oblique incidence case as indicated in the figure. Fig. 3(b) shows the reassigned spectrogram of the same broadband data. Again, it is observed that the precision of the signal components is enhanced, thus leading to improved readability of the spectrogram when compared to the STFT spectrogram. Note, however, that the resolution of the reassigned transform is still limited by the Fourier uncertainty bounds. For instance, it is possible to perfectly resolve two modes only as long as they are further apart than σ along the time axis and $1/\sigma$ along the frequency axis. In the figure, it is observed that when the modal lines are very close (within the Fourier limits), they are not perfectly resolved either by the STFT or the RJTF implementations. Thus, the RJTF achieves optimal precision but does not achieve better resolution than the STFT.

Broadband (1–18 GHz) measurements of the open waveguide returns are next made in the laboratory using a vector network analyzer and two broadband horn antennas. The broadband S_{21} measurement of the background (without the target) is subtracted from the target return to reduce the effect of the background and the direct coupling between the horns. Fig. 4(a) shows the STFT of the target returns for normal incidence. The spectrogram shows good agreement with the simulation results. However, there are some important differences. First, a second vertical line, labeled as 3, occurs at an additional roundtrip delay of 4.1 ns after the rim return. It is caused by the

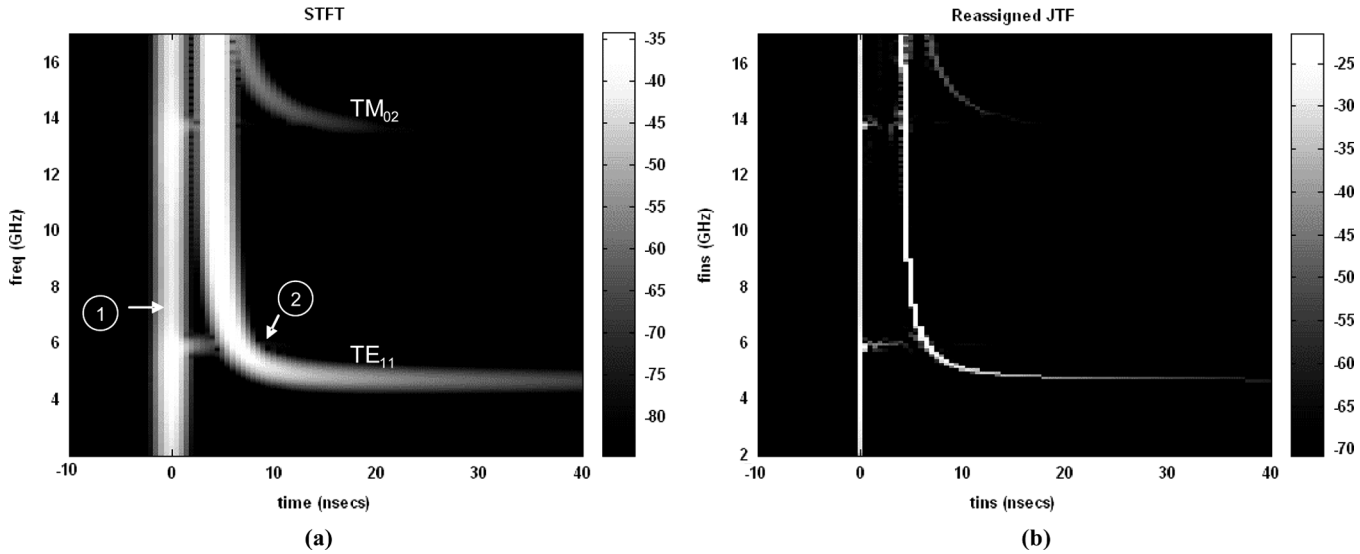

Fig. 2. Joint time-frequency representation of simulated scattered field from a circular waveguide cavity for 0° incidence using (a) STFT and (b) RJTF transform.

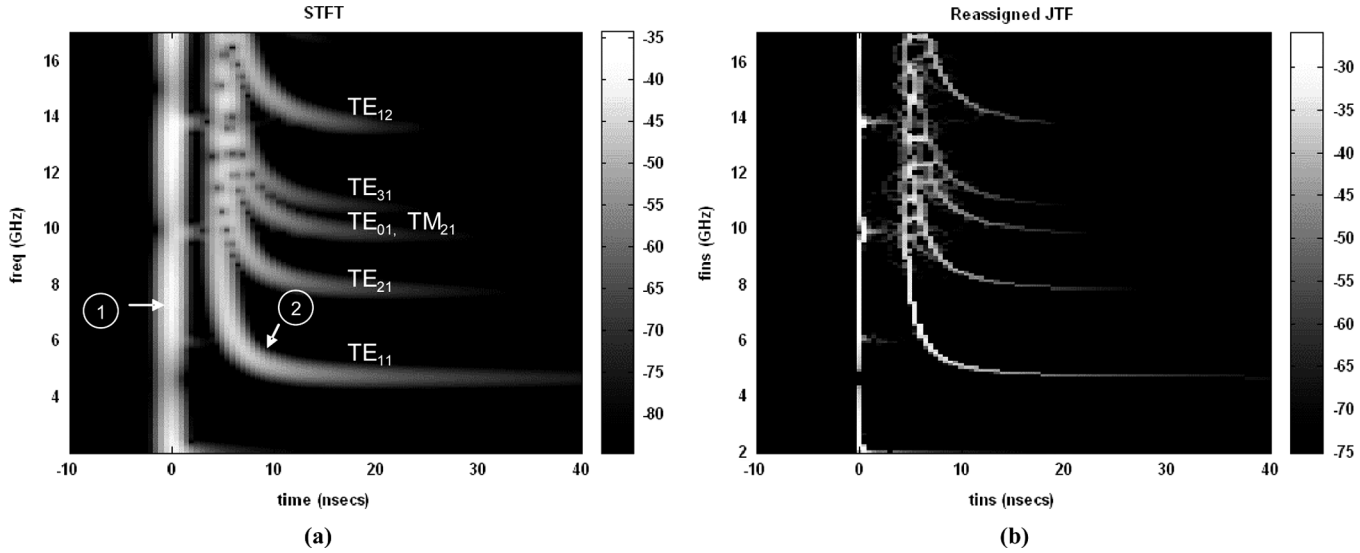

Fig. 3. Joint time-frequency representation of simulated scattered field from a circular waveguide cavity for 45° vertically polarized incidence using (a) STFT and (b) RJTF transform.

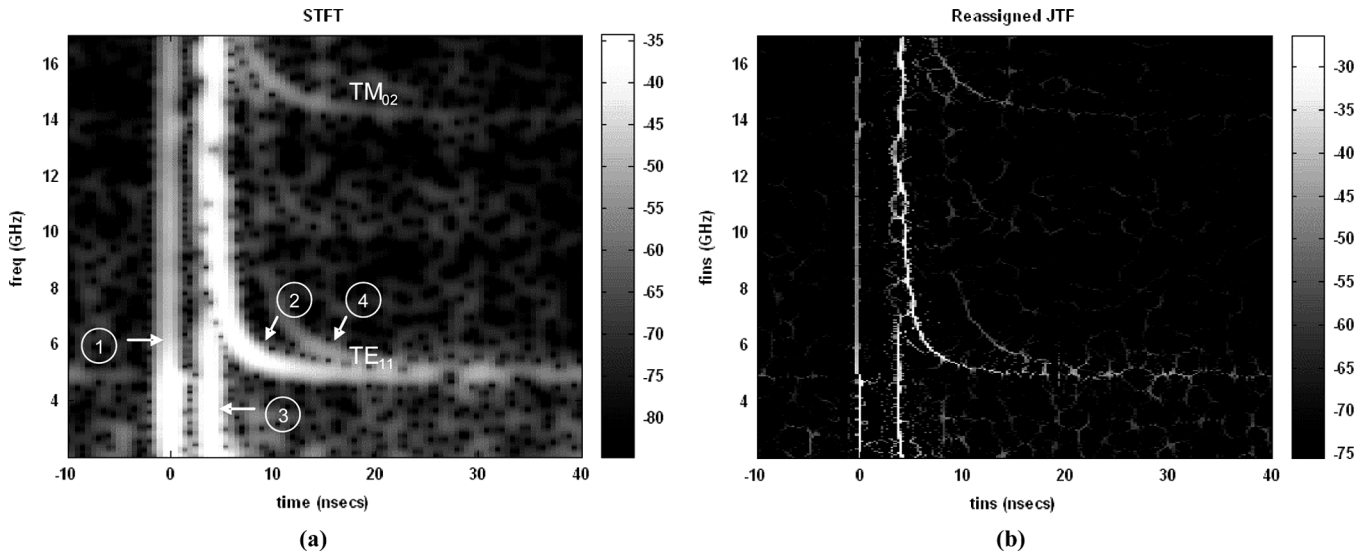

Fig. 4. Joint time-frequency representation of measured scattered field from a circular waveguide cavity for 0° incidence using (a) STFT and (b) RJTF transform.

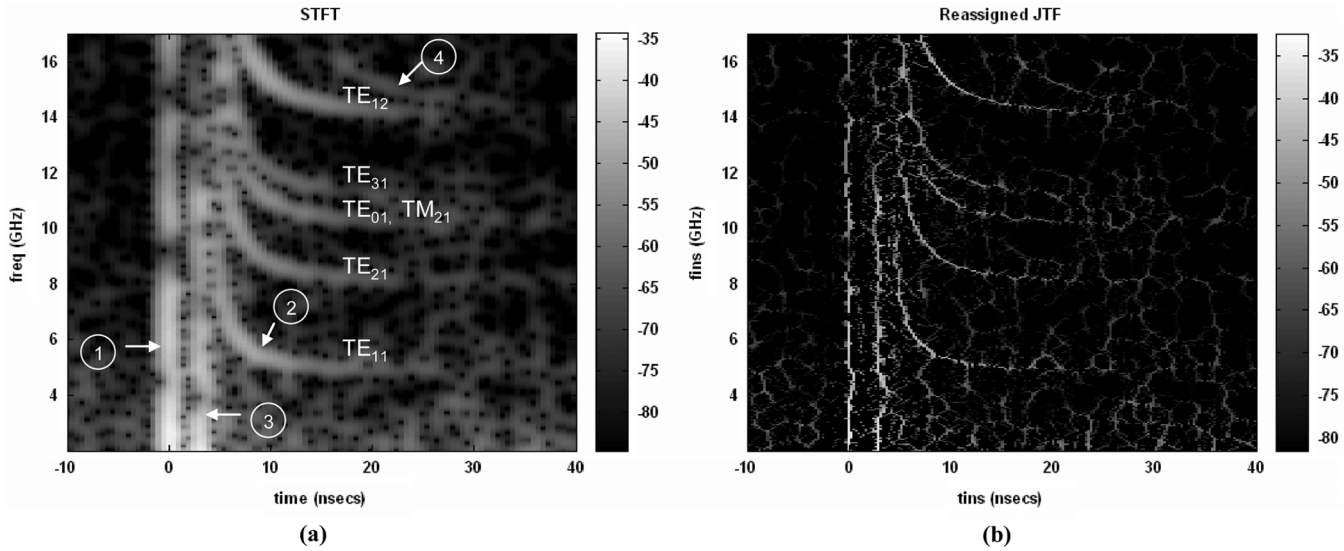

Fig. 5. Joint time-frequency representation of measured scattered field from a circular waveguide cavity for 45° vertically polarized incidence using (a) STFT and (b) RJTF transform.

scattering from the exterior back end of the cavity. Second, another new feature that is observed in the spectrogram, labeled as 4, is the scattering from the interior after a two-roundtrip travel within the cavity. This mechanism was not accounted for in the modal simulation, which only included the single-roundtrip return. Fig. 4(b) shows the reassigned spectrogram of the same data. It shows improved precision of the signal energy in the time and frequency domains. The underlying noise is localized into a "froth-like" pattern. This is similar to the reassigned spectrogram of white Gaussian noise reported in [7]. It is observed that in the areas where the signal-to-noise ratio (SNR) is high, the signal lines dissociate from the underlying froth patterns. A moderate improvement in the SNR of the RJTF distribution is observed in comparison to the STFT distribution.

Fig. 5(a) and (b) shows the time-frequency plots obtained by the application of the STFT and the reassigned transform on the target returns obtained for a 45° vertical polarized incident wave. Both plots show good agreement with the simulation results presented earlier, except for the addition of mechanisms 3 and 4. Superior precision is achieved in the reassigned spectrogram when compared to the STFT spectrogram.

IV. Conclusion

The application of the RJTF transform on broadband scattering data from an open-ended waveguide cavity has been investigated. The implementation of the reassigned distribution has been derived for a frequency domain signal and its characteristics have been studied in relation to the conventional STFT. The reassigned transform achieves improved signal localization in the time and frequency domains when compared to the STFT. The resolution, however, remains the same. Noise is localized into a froth-like pattern and a moderate improvement in the SNR is observed in the reassigned spectrogram. This transform is well suited when the STFT does not provide sufficient localization of the signal features of interest. We have recently applied this transform to study the micro-Doppler returns from human movements. In that case, many different time-varying Doppler features due to the dynamics of the different body parts are manifested in the time-frequency plane. The results will be reported elsewhere [10].

References

[1] V. C. Chen and H. Ling, *Time Frequency Transforms for Radar Imaging and Signal Analysis*. Boston, MA: Artech House, 2002.
[2] A. Moghaddar and E. K. Walton, "Time-frequency distribution analysis of scattering from waveguide cavities," *IEEE Trans. Antennas Propag.*, vol. 41, no. 5, pp. 677–680, May 1993.
[3] H. Kim and H. Ling, "Wavelet analysis of radar echo from finite-size targets," *IEEE Trans. Antennas Propag.*, vol. 41, no. 2, pp. 200–207, Feb. 1993.
[4] K. Kodera, C. De Villedary, and R. Gendrin, "Analysis of time varying signals with small BT values," *IEEE Trans. Acoust. Speech Signal Process.*, vol. ASSP-26, no. 1, pp. 64–76, Feb. 1978.
[5] F. Auger and P. Flandrin, "Improving the readability of time frequency and time scale representations by the reassignment method," *IEEE Trans. Signal Process.*, vol. 43, no. 5, pp. 1068–1089, May 1995.
[6] S. A. Fulop and K. Fitz, "Algorithms for computing the time-corrected instantaneous frequency (reassigned) spectrogram, with applications," *J. Acoust. Soc. Amer.*, vol. 119, no. 1, pp. 360–371, Jan. 2006.
[7] T. J. Gardner and M. O. Magnasco, "Sparse time-frequency representations," in *Proc. Nat. Acad. Sci.*, Apr. 2006, vol. 103, no. 16, pp. 6094–6099.
[8] H. Ling, S. W. Lee, and R. Chou, "High-frequency RCS of open cavities with rectangular and circular cross sections," *IEEE Trans. Antennas Propag.*, vol. 37, no. 5, pp. 648–654, May 1989.
[9] C. A. Chuang, C. S. Liang, and S. W. Lee, "High-frequency scattering from an open-ended semi infinite cylinder," *IEEE Trans. Antennas Propag.*, vol. AP-23, no. 6, pp. 770–776, Nov. 1975.
[10] S. S. Ram and H. Ling, "Analysis of microDopplers from human gait using reassigned joint time- frequency transform," *Electron. Lett.*, May 2007, submitted for publication.